infrastructures

MDPI

Article

Mechanical Performance, Durability, and Environmental Assessment of Low-Carbon Fiber-Reinforced Reactive Powder Concrete with a High Content of Fly Ash

Ying Peng [1], Nida Chaimoon [2], Yike Wu [3], Yuanfeng Chen [3] and Krit Chaimoon [1,*]

[1] Structural Engineering Research Unit, Faculty of Engineering, Mahasarakham University, Kham Riang, Maha Sarakham 44150, Thailand
[2] Water Resources and Environmental Engineering Research Unit & Circular Resources and Environmental Protection Technology Research Unit, Faculty of Engineering, Mahasarakham University, Kham Riang, Maha Sarakham 44150, Thailand
[3] College of Civil Engineering, Putian University, Putian 351100, China
* Correspondence: k.chaimoon@msu.ac.th

Abstract

Reactive powder concrete (RPC) delivers outstanding mechanical performance and durability; however, it is commonly hindered by high cement consumption, elevated embodied carbon emissions, and high material costs. To mitigate these drawbacks, this study develops a low-carbon, cost-effective RPC incorporating high-volume class-F fly ash, a reduced silica fume dosage, conventional river sand, and an optimized steel fiber system. A systematic mix design framework, combining particle packing density with paste rheology optimization, was employed to balance workability, strength, and durability. The optimized mixtures were evaluated for compressive, splitting tensile, and flexural strength, as well as durability-related metrics, including water absorption rate and resistance to chloride penetration. Environmental impact and cost-effectiveness were further quantified via embodied carbon accounting and strength-normalized performance indices. The results show that well-designed high-volume fly ash RPC can achieve compressive strengths above 130 MPa while maintaining excellent impermeability, alongside substantial reductions in both material cost and carbon footprint relative to conventional RPC. In addition, mixed-size steel fibers further enhance mechanical performance through multi-scale crack bridging. Overall, this work provides a practical route to decouple ultra-high performance from high environmental burden, supporting the sustainable deployment of RPC in infrastructure engineering.

Keywords: reactive powder concrete; waste; fly ash; durability; low-carbon concrete

Check for updates

Academic Editor: Md. Safiuddin

Received: 21 January 2026
Revised: 4 March 2026
Accepted: 9 March 2026
Published: 11 March 2026

Copyright: © 2026 by the authors. Licensee MDPI, Basel, Switzerland. This article is an open access article distributed under the terms and conditions of the Creative Commons Attribution (CC BY) license.

1. Introduction

Reactive powder concrete (RPC) represents an advanced class of cement-based composites distinguished by ultra-high strength, an exceptionally dense microstructure, and superior durability. By eliminating coarse aggregates and employing finely graded powders at very low water-to-binder ratios, RPC can achieve compressive strengths above 120 MPa while maintaining excellent resistance to aggressive exposures, including chloride ingress, sulfate attack, and severe thermal conditions [1–4]. Such performance is commonly attributed to the synergistic effects of optimized particle packing, refined pore architecture, and efficient crack bridging provided by steel fiber reinforcement, which together suppress permeability and delay damage localization [5,6].

Notwithstanding these advantages, the broader adoption of RPC in large-scale infrastructure is still limited by its high cost and substantial environmental burden. Conventional RPC typically relies on very high cement contents, coupled with significant silica fume and steel fiber dosages, which increase embodied carbon and undermine economic feasibility [7,8]. Against the backdrop of global decarbonization targets and increasingly stringent sustainability requirements, the development of low-carbon RPC that retains ultra-high performance while reducing clinker dependency has become a pressing research priority. Importantly, decarbonizing RPC is not a straightforward cement-replacement exercise, because its hallmark performance is governed by a tightly coupled system involving particle packing, paste rheology, hydration kinetics, and fiber–matrix interfacial synergy [9].

Supplementary cementitious materials (SCMs) offer a well-established pathway to reduce cement demand and associated emissions in high-performance cementitious systems. Among them, fly ash is particularly attractive, owing to its widespread availability, spherical particle morphology, and latent pozzolanic reactivity. In ultra-dense, low-water-to-binder matrices such as RPC, the influence of fly ash is inherently multi-scale and extends beyond the simple dilution of clinker: (i) at the particle level, the "ball-bearing" effect and micro-filler action can improve flowability and packing density, thereby lowering pore connectivity; (ii) at the kinetics/chemistry level, class-F fly ash typically slows early hydration but contributes to later-age densification through secondary reactions and pore refinement; and (iii) at the interfacial level, fly ash-induced changes in hydrate assemblage and pore solution chemistry may alter fiber–matrix bond development and the crack-bridging law that governs splitting tensile and flexural behavior. Consequently, the optimal fly ash content in RPC should be determined by a coupled optimization of rheology, densification, and fiber-bridging efficiency rather than compressive strength alone.

However, implementing high-volume fly ash (HVFA) in RPC remains technically complex. At high replacement levels, fly ash's slower reaction kinetics can delay early hydration, impede early-age strength development, and postpone microstructural densification under conventional curing regimes [10]. This may further manifest as insufficient early matrix stiffness for effective fiber anchorage, increased risk of fiber segregation if yield stress is not properly controlled, and delayed impermeability development if packing and paste stability are not adequately engineered.

Recent multiple-scale investigations in low-carbon cementitious composites provide additional theoretical support for the above coupling. Zhou et al. (2025) examined slag-based engineered geopolymer composites with varying fly ash contents using single-fiber pull-out, single-crack tensile, and dog-bone tensile tests and reported that increasing fly ash content can markedly enhance tensile and flexural performance together with the maximum bridging stress, which was associated with fly ash-driven changes in matrix phase assemblage and fiber–matrix interfacial properties evidenced by microstructural characterization [11]. Although geopolymer matrices differ from Portland-cement-based RPC, the central implication is transferable: fly ash can reconfigure the interfacial contact state and thus reshape the bridging law governing crack spacing and crack opening evolution. Therefore, developing HVFA-RPC with ultra-high performance requires explicit design of paste rheology for fiber dispersion and matrix chemistry/densification for robust interfacial bonding, rather than relying solely on later-age pozzolanic strength gain.

Recent progress in fracture mechanics further underscores that strength-based metrics alone are insufficient to capture the structural performance of ultra-high-performance fiber-reinforced cementitious composites. Analytical descriptions that account for crack evolution and fiber-bridging mechanisms are increasingly used to interpret size-dependent and post-cracking behavior. For example, Kumar et al. [12] proposed an analytical framework linking load–CMOD responses with multi-stage tensile constitutive assumptions,

offering mechanistic insight into microcracking and bridging-dominated stages. Nevertheless, whether such mechanistic interpretations and their underlying fiber-bridging concepts remain transferable to low-carbon RPC incorporating HVFA and multi-scale fiber configurations is still not well-established, especially when the matrix chemistry, interfacial properties, and rheology are intentionally modified to reduce clinker content.

Moreover, in fiber-reinforced RPC, performance is governed not only by matrix strength but also by fiber dispersion, interfacial bond development, and multi-scale crack-bridging efficiency—features that may be altered when fly ash modifies the paste rheology and hydration products [13]. Consequently, the coupling between fly ash-modified matrices and steel fiber reinforcement remains insufficiently clarified, despite its direct relevance to splitting tensile and flexural behavior as well as post-cracking capacity. In this context, HVFA may amplify the sensitivity of mechanical response to rheological stability and interfacial evolution, making unified mix design and fiber optimization particularly necessary.

Steel fibers are central to achieving the ductility and damage tolerance that distinguish RPC from brittle ultra-dense cementitious matrices. Experimental evidence indicates that the fiber length, dosage, and size distribution strongly influence tensile response, flexural strength, and post-peak energy dissipation by controlling crack initiation, crack spacing, and bridging stress transfer [14]. In particular, mixed-size (hybrid) fiber systems can activate crack bridging across multiple length scales, improving resistance to both microcrack coalescence and macrocrack opening. However, the combined effects of optimized fiber systems and fly ash incorporation on mechanical performance, durability indices, and sustainability outcomes have rarely been examined in a unified design framework.

Accordingly, this study aims to develop a low-carbon and cost-effective fiber-reinforced RPC incorporating high-volume class-F fly ash, reduced silica fume dosage, conventional river sand, and an optimized steel fiber system. A systematic mix design methodology is adopted in which particle packing density and paste rheology are co-optimized to achieve superior fresh-state performance while enabling substantial clinker reduction. The mechanical properties (compressive, splitting tensile, and flexural strength) and durability-related indicators (water absorption rate and resistance to chloride penetration) are comprehensively evaluated, and environmental and economic performance are quantified using embodied carbon emissions, material cost, and strength-normalized performance indices. The central innovation is a unified performance–sustainability design framework that couples packing–rheology control (to make HVFA workable and structurally dense) with hybrid fiber optimization (to restore and enhance multi-scale crack bridging), thereby enabling 130 MPa-class strength and excellent impermeability while simultaneously reducing carbon footprint and cost. The results are expected to provide practical guidance for sustainable RPC design and accelerate the engineering deployment of low-carbon RPC in modern infrastructure.

2. Experimental Details

2.1. Materials

The cementitious materials (binder) consisted of cement (C), silica fume (SF), and class-F fly ash (FFA). The cement was a hydraulic low-carbon cement manufactured in Thailand, compliant with TIS 2594-2556 [15] (performance-based specification referencing ASTM C1157), and reported to emit approximately 10.2% less CO_2 than ordinary Portland cement [16–18]. The SF was supplied by Elkem Company, Thailand, in undensified form with a specific surface area of 15.0–35.0 m^2/g and a bulk density of 500–700 kg/m^3. The FFA complied with ASTM C618 [19] (class F) and was sourced in Thailand. By XRF, the chemical compositions of C, SF, and FFA are summarized in Table 1. River sand collected

from the Chi River (Thailand) was used as fine aggregate; its properties and appearance are presented in Figure 1. The sand was used in saturated surface-dry (SSD) condition. An SSD moisture content of 0.3% was adopted for water correction when dry sand was used. The particle size distribution curves of the binder components are presented in Figure 2. A polycarboxylate-based superplasticizer (SP) was used to achieve adequate flowability at low water content.

Table 1. Chemical compositions of binding materials (wt.%).

Chemical Composition	C	SF	FFA
SiO_2	13.32	94.8	53.03
Al_2O_3	2.73	0.15	16.97
Fe_2O_3	3.54	0.03	6.22
CaO	74.37	0.88	15.69
MgO	0.89	0.70	0.78
SO_3	3.50	0.96	4.09
Na_2O	0.28	0.20	0.35
K_2O	0.49	1.98	1.27
TiO_2	0.26	0.00	0.98
LOI	0.12	0.01	0.01

Note: LOI—loss of ignition.

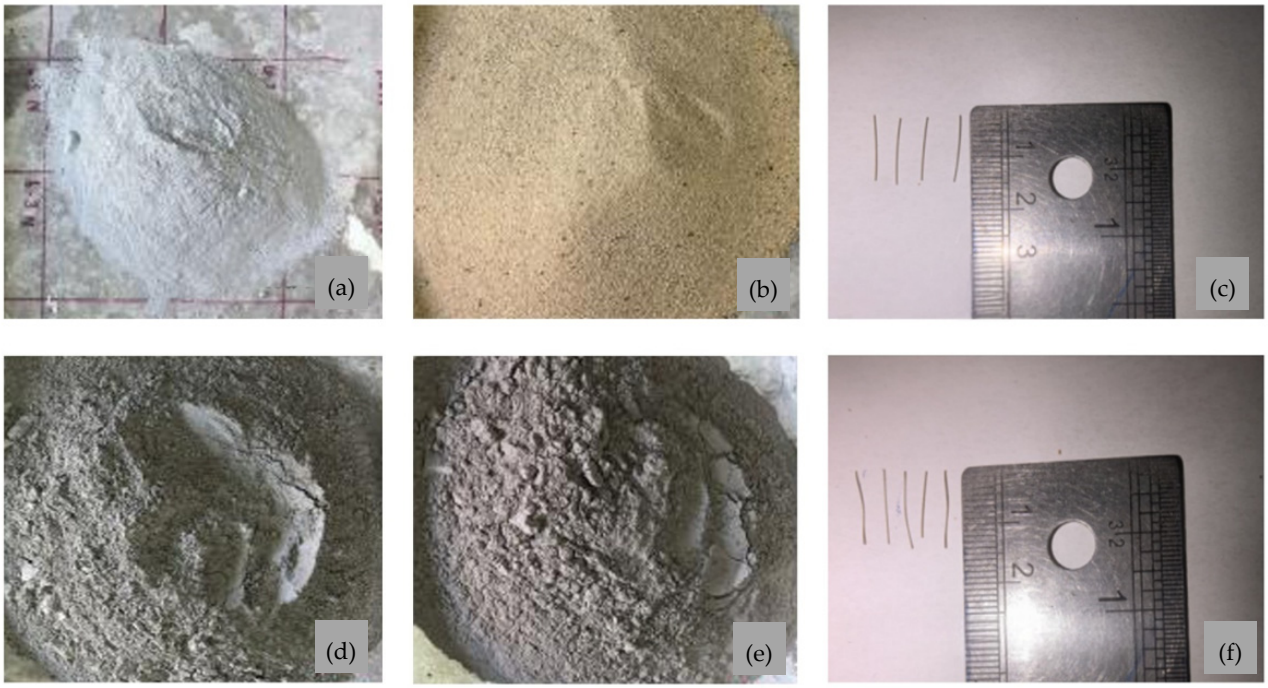


Figure 1. Raw materials: (**a**) Silica fume; (**b**) sand; (**c**) single-size steel fiber; (**d**) cement; (**e**) class-F fly ash; (**f**) mixed-size steel fiber.

Straight, brass-coated micro steel fibers sourced from China and compliant with JT/T 524 [20] were used. Two fiber systems were considered: a single-size steel fiber (SSTF; 0.22 mm diameter, 13 mm length; aspect ratio 59) and a mixed-size steel fiber (MSTF; 0.18–0.35 mm diameter, 12–14 mm length; tensile strength 2850 MPa; aspect ratio 37–78, average 56), both shown in Figure 1. The MSTF size range was selected to enable multi-scale crack bridging in RPC: finer fibers increase fiber number density and improve microcrack control, whereas relatively coarser fibers provide higher pull-out resistance at larger crack openings. The narrow length range (12–14 mm), consistent with commercially available products meeting JT/T 524, was adopted to maintain mixing feasibility and limit fiber

balling and workability loss in ultra-low-w/b RPC. According to supplier quotations, MSTF provided approximately a 44% cost reduction relative to SSTF.

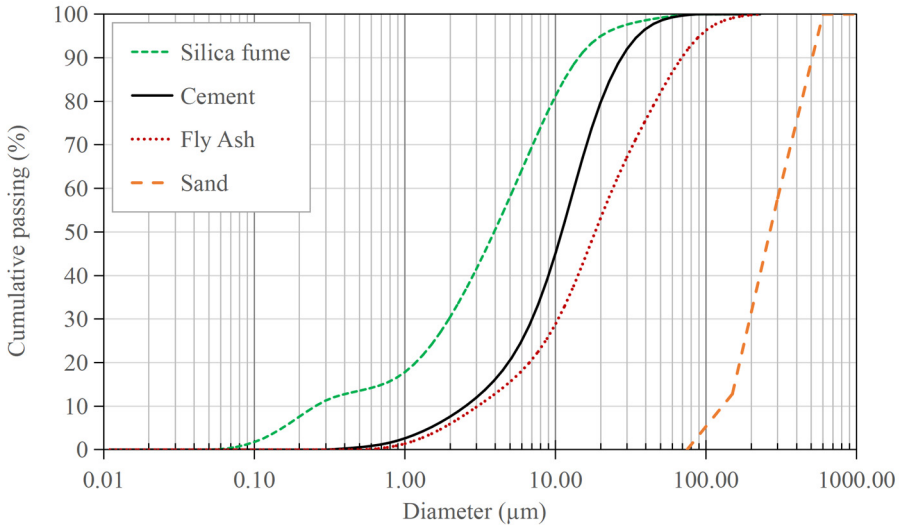


Figure 2. The particle size distribution curves of the binder components.

2.2. Sample Preparation

2.2.1. Mix Design

A systematic five-step mix design strategy [21] was adopted to develop a low-carbon RPC with high-volume SCM incorporation while maintaining fresh-state workability and high hardened performance: optimizing the binder combinations at the paste level, selecting the w/b, selecting the sand, determining the cementitious-material-to-sand mass ratio (M_{cm}/M_s), and determining the fiber content.

Step 1: Optimize the binder combinations at the paste level

A paste-first design strategy [21] was adopted because under fixed sand grading and fiber dosage the rheology and packing efficiency of the binder matrix predominantly govern both the fresh and hardened performance of RPC [1–3]. To reduce cost, the binder design emphasized high-volume class-F fly ash (FFA) with a reduced silica fume (SF) content; the preliminary binder space covered SF contents of 2–19% and FFA contents of 27–61% by mass (see Table 2). Mini-slump tests were conducted following ASTM C1437 [22] using paste mixtures with water-to-binder ratios ranging from 0.40 to 1.00 (by mass) to quantify flow behavior and water demand. From the linear relationship between the flow spread and water-to-binder ratio, the intercept was defined as the minimum water content (MWC) required to initiate flow and the slope as the relative water demand (RWD). Assuming negligible air entrainment, a lower MWC indicates a smaller minimum void volume and thus higher packing density, which is favorable for achieving high strength and durability in ultra-dense matrices [16]. Binder systems (see Figure 3) exhibiting low MWC and favorable RWD were further screened using 2- and 28-day compressive strength (ASTM C109) [23], mini-slump flow, and mini-V-funnel flow time tests. The superplasticizer (SP) dosage was adjusted to achieve a target flow diameter of 300–350 mm, and mixtures providing higher strength at lower SP demand were prioritized. A multi-criteria radar-chart analysis was employed to balance the MWC, RWD, SP dosage, and compressive strength (at 2 and 28 days), where data were normalized and reciprocal transformation was applied to negative metrics so that larger radar areas correspond to better overall performance.

Table 2. Binder combinations (wt.%).

Number	Group	Code	Cement	FFA	SF
1	1	C100	100	0	0
2	2	C73F27	73	27	0
3		C64F36	64	36	0
4		C54F46	54	46	0
5		C49F51	49	51	0
6		C44F56	44	56	0
7		C39F61	39	61	0
8	3	C98S2	98	0	2
9		C96S4	96	0	4
10		C92S8	92	0	8
11		C89S11	89	0	11
12		C85S15	85	0	15
13		C81S19	81	0	19
14	4	C66F32S2	66	32	2
15		C64F32S4	64	32	4
16		C60F32S8	60	32	8
17		C61F37S2	61	37	2
18		C59F37S4	59	37	4
19		C55F37S8	55	37	8
20		C56F42S2	56	42	2
21		C54F42S4	54	42	4
22		C50F42S8	50	42	8



Figure 3. Experimental procedures of mini-slump flow test and mini-V-funnel test.

Step 2: Select the w/b

Based on the SP demand and the standard 28-day compressive strength development, the water-to-cementitious-material ratio was selected as w/b = 0.18, which falls within the typical RPC range of 0.15–0.25 [17]. This w/b was then fixed and applied in subsequent mortar- and fiber-reinforced RPC optimization stages to ensure comparability across sand and fiber variables.

Step 3: Select the sand

To reduce production cost relative to conventional RPC that relies on specialty ultra-fine sand, a traditional river sand commonly used in construction was adopted. The sand was characterized in SSD condition, and its SSD moisture content was measured as 0.3% for water correction when dry sand was used.

Step 4: Determine the M_{cm}/M_s

The cementitious-material-to-sand mass ratio (M_{cm}/M_s) was selected to ensure sufficient filling and coating capacity of the optimized paste for the chosen sand. Based on a study by Meng et al. [21], M_{cm}/M_s = 1.2 was adopted.

Step 5: Determine the fiber system and fiber content

Fiber optimization was conducted within a practical RPC range using MSTF at volume fractions of 2.0%, 1.5%, and 1.0% (see Table 3). To ensure fresh-state comparability, mini-slump flow was controlled at 250 ± 20 mm by adjusting the SP dosage, and the flexural response at 28 days was evaluated following ASTM C1609. The final mixture selection targeted a 28-day compressive strength exceeding 120 MPa under standard curing.

Table 3. Optimize fiber volume for RPC (kg/m^3).

No. 14	V_f (%)	C	FA	SF	W	S	MSTF	SP	Extra Water
C66F32S2MSTF	2.0	728.44	349.65	20.35	197.72	906.5	157	45	2.72
	1.5						117.75	40	
	1.0						78.5	40	

2.2.2. Mixing, Casting, and Curing Procedure

All mixtures were prepared at room temperature (25 ± 3 °C) using a 150 L mixer manufactured by Eirich Co., Ltd. (Shanghai, China). A double-batch mixing procedure was adopted to enhance dispersion under low-w/b conditions: all binders (C, SF, FFA) were first dry-mixed with sand, after which half of the dry blend was mixed with half of the premixed liquid (water and SP) until homogenized; the remaining dry blend and remaining premixed liquid were then added and mixed to homogeneity; finally, steel fibers were introduced at the end of the final mixing stage and mixed until uniformly dispersed. Specimens were cast in a single lift without mechanical consolidation, immediately sealed with plastic wrap after casting, demolded after 24 h, and water-cured at 25 ± 3 °C until the designated testing ages. Each mixture contains four parallel samples, whilst the average value plus the standard deviation are presented.

2.3. Testing

The mini-slump flow test (see Figure 3) was used to quantify the flowability of the cementitious paste and to determine the MWC and RWD for each binder combination. All of the constituents (cement and supplementary cementitious materials) were first weighed to the target proportions. Mixing was conducted using a 5 L laboratory mixer manufactured by Bossen Co., Ltd. (Rayong, Thailand): the dry powders were blended to homogenize, after which pre-measured mixing water (and superplasticizer when applicable) was added, and the paste was mixed until a uniform, lump-free consistency was obtained. Immediately

after mixing, the mini-slump cone (bottom opening diameter D1 = 100) was placed on a clean, non-absorbent plate and filled in one lift; the surface was leveled by striking off without external vibration. The cone was then lifted vertically in a steady motion to allow free spreading. After the flow ceased, two orthogonal spread diameters were measured and averaged to obtain D2. The relative flow was calculated as (D2 − D1)/D1. For each binder system, a series of pastes with different w/b ratios was tested, and a linear relationship between w/b (*y*-axis) and relative flow (*x*-axis) was established; the intercept was taken as the MWC and the slope as the RWD [21]. Measurements were performed at least twice for each mixture, and the apparatus was cleaned and dried between tests to avoid cross-contamination.

The mini-V-funnel test (see Figure 3) was performed to assess the flow time of the fresh cementitious paste/mortar as an indicator of viscosity and passing ability under gravity-driven discharge. All of the materials (water, cement, fly ash, silica fume, and superplasticizer where used) were weighed according to the mix design. Prior to testing, the mini V-funnel was cleaned and lightly moistened; the discharge gate was closed and checked for leakage. The fresh mixture was poured into the funnel promptly and the top surface was leveled. The gate was then opened, and the discharge time (in seconds) was recorded from gate opening until the continuous outflow ceased (i.e., the funnel was effectively emptied). The test was repeated to confirm repeatability, and the funnel was thoroughly cleaned between runs. The measured V-funnel time was used to compare mixtures in terms of fresh rheological resistance to flow, with longer times indicating higher apparent viscosity and/or reduced flowability under self-weight.

Mechanical properties were evaluated using standard methods across designated ages. Compressive strength was measured on 50 × 50 × 50 mm cubes in accordance with ASTM C109 at 1, 3, 28, 56, and 90 days. Splitting tensile strength was determined following ASTM C496 [24] using Ø100 × 200 mm cylinders at 28 days. Flexural performance was assessed at 28 days using 75 × 75 × 280 mm prisms in accordance with ASTM C78 [25], enabling characterization of first-crack strength and post-cracking load-carrying capacity via load–deflection response. For microstructural characterization, fractured and polished specimens were observed using a scanning electron microscope (SEM) after vacuum drying and gold sputter coating. The observations were conducted under a secondary electron (SE) mode with an accelerating voltage of 15 kV, at various magnifications. Durability-related transport indicators included resistance to chloride penetration and water absorption rate. Chloride resistance was evaluated using the rapid chloride penetration test (ASTM C1202) [26] by applying a 60 V potential for 6 h on saturated specimens and recording the total charge passed, where a lower charge indicates a denser microstructure and superior impermeability; specimens were demolded at 24 h, water-cured for 28 days, and then tested. Water absorption rate was measured following ASTM C1585 [27] using Ø100 × 200 mm cylinders that were water-cured for 28 days and sectioned into 50 ± 3 mm slices; specimens were dried at 50 ± 2 °C for 3 days, vacuum-sealed for 15 days to stabilize moisture, coated to ensure one-dimensional ingress, and tested at 25 ± 2 °C, with mass recorded at predefined intervals to compute sorptivity. Lower sorptivity indicates a more compact pore network and improved resistance to fluid-mediated deterioration mechanisms.

3. Results and Discussion

3.1. Optimization of Binder and Fiber Combinations

3.1.1. Selection of Binder Materials

Under negligible air entrainment, a lower MWC indicates a smaller minimum void volume and thus a higher packing density of the binder system, which is beneficial for strength and impermeability [28]. In contrast, a lower RWD implies that the paste's

fluidity is less sensitive to changes in water content, reflecting an improved rheological property under the low-w/b regime typical of RPC; therefore, the desirable binder system is characterized by a low MWC and a low RWD. The results presented in Figure 4 reveal clear effects of SCM type and dosage on these two descriptors. In binary cement–fly ash systems, increasing the content of class-F fly ash generally reduced the MWC, consistent with its spherical morphology and micro-filling/lubrication effects that enhance packing efficiency; the mix with the highest fly ash content (i.e., C39F61) achieved one of the lowest MWC values, confirming that HVFA can lower the minimum water requirement for flow initiation. By contrast, binary cement–silica fume systems tended to increase MWC at higher silica fume contents, which is attributable to the extremely fine particle size and high surface area of silica fume that increases water demand through adsorption and flocculation tendencies. Importantly, ternary systems exhibited a synergy: mixes combining HVFA with a small amount of silica fume simultaneously achieved a low MWC and improved stability, indicating that an appropriately dosed silica fume fraction can "complete" the particle size spectrum and reduce voids beyond what fly ash alone can deliver. Across the ternary groups, a silica fume content around 4% repeatedly produced more favorable MWC–RWD combinations than 2% or 8%, suggesting an optimal balance between packing enhancement (filler effect) and rheological penalty (surface adsorption). This observation provides the quantitative basis for moving from broad binder screening to a multi-criteria selection that also accounts for hardened performance.

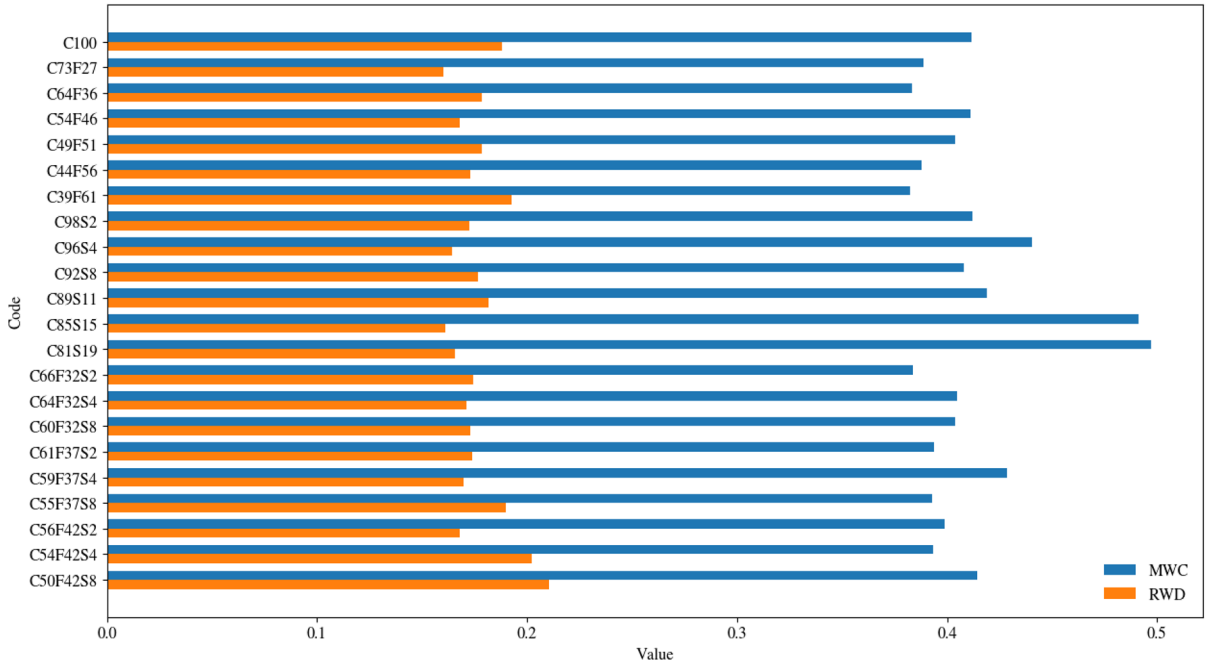


Figure 4. Effect of binder type on the minimum water content (MWC) and relative water demand (RWD).

3.1.2. Narrowing Binder Materials

Because paste flow descriptors alone do not guarantee adequate strength development, shortlisted binders from the MWC–RWD screening were further evaluated by integrating fresh-state demand and early/standard strength metrics. Specifically, the assessment considered MWC, RWD, SP demand (to reach the target flow diameter), flow time (as an indicator of viscosity/stability), and compressive strength development at early age and 28 days. These competing criteria were synthesized using a radar-chart approach (see Figure 5), where each variable was normalized and weighted to reflect the design intention of achieving both workable self-compacting behavior and sufficient early strength for

practical applications. In this framework, binder systems that require less water and less SP to attain stable flow, while simultaneously delivering higher compressive strength, achieve a larger enclosed radar area and are therefore considered more balanced candidates [29]

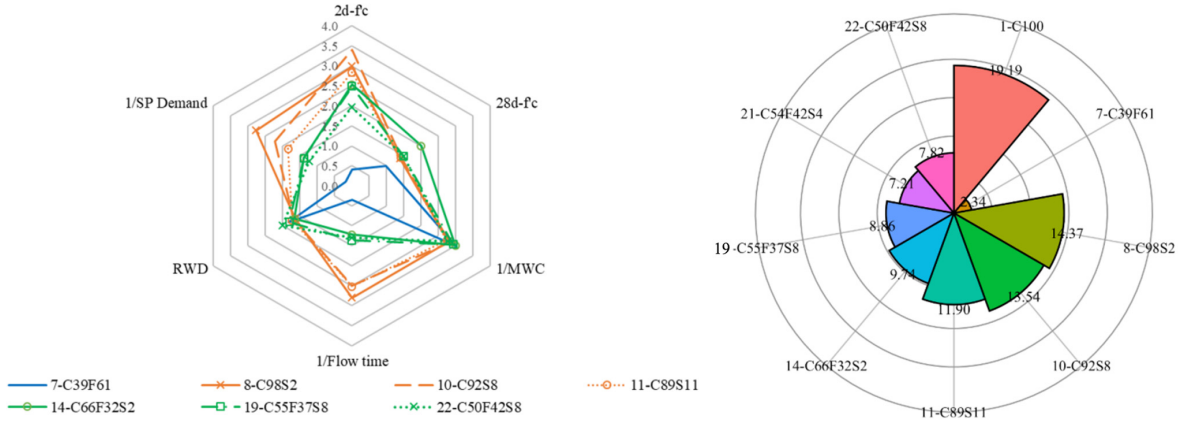


Figure 5. Multi-criteria performance comparison of mixtures: radar plots of normalized indices (**left**); radar-chart area as a composite performance score (**right**).

The radar analysis identifies a small set of mixtures that provide superior overall trade-offs and, importantly, it separates the "conventional strength-driven" and "sustainability-driven" design options. Mix No. 10 (C92S8) represents a high-cement, silica fume-enhanced route that typically supports strong early densification. Mix No. 14 (C66F32S2), in contrast, embodies the targeted low-carbon strategy by combining high-volume fly ash with minimal silica fume while still maintaining competitive rheology and strength potential. Therefore, these two binders were retained as representative systems for comparative discussion; however, for subsequent fiber optimization and full RPC validation, Mix No. 14 was prioritized because it aligns with the study's primary objective of reducing clinker and silica fume consumption while sustaining high-performance potential [30]

3.1.3. Determination of Fiber Content

Based on the paste optimization and multi-criteria evaluation, Mix No. 14 was selected as the reference matrix for fiber optimization. The fiber study focused on MSTF at volume fractions of 1.0%, 1.5%, and 2.0% because a hybrid size distribution is expected to improve crack-bridging efficiency across multiple length scales while offering cost advantages relative to single-size fibers. Fresh-state control was implemented by adjusting SP to achieve a comparable mini-slump flow level (targeting approximately 270 ± 20 mm), while mixing time was monitored as a practical indicator of dispersion difficulty and potential fiber congestion. As shown in Figure 6, increasing the fiber volume from 1.5% to 2.0% noticeably increased both SP demand and mixing time, reflecting a rapid rise in rheological resistance and dispersion difficulty at higher fiber contents. This fresh-state penalty is not merely a processing inconvenience; it is mechanistically linked to the risk of fiber clustering, entrapped air, and local heterogeneity, which can ultimately reduce compressive strength and increase variability [31] On this basis, the three MSTF mixtures (1%, 1.5%, and 2%) were carried forward to mechanical verification and an additional 1.5% SSTF mixture was included as a control for isolating the effect of fiber size distribution.

3.2. Mechanical Properties

Figure 7 shows that the compressive strength response is strongly dependent on fiber dosage and fiber configuration, but in a non-monotonic manner. Among the MSTF mixtures, 1.5% MSTF (M14-2B) delivered the best overall performance, achieving

135.42 MPa at 28 days and continuing to increase to 140.31 MPa at 90 days, while maintaining acceptable variability. In contrast, increasing the fiber dosage to 2.0% MSTF (M14-2C) led to a marked reduction in compressive strength at early age and at 28 days (e.g., 94.17 MPa at 28 days), despite the higher nominal fiber content. This inversion indicates that, beyond an optimal fiber volume, the detrimental effects of reduced workability and impaired dispersion outweigh the potential benefit of additional crack arresters. The increased SP demand and prolonged mixing time observed for 2.0% MSTF support this interpretation, as these conditions are conducive to fiber congestion and air entrapment, both of which compromise the effective load-bearing continuity of an ultra-dense matrix. The 1.0% MSTF mixture (M14-2A) shows intermediate behavior, suggesting that it does not provide sufficient reinforcement efficiency to fully exploit the matrix potential, whereas 1.5% MSTF achieves an effective balance between dispersion feasibility and reinforcement contribution. Comparison with the SSTF control further clarifies the role of fiber gradation. The 1.5% SSTF mixture (M14-1) exhibits a lower 28-day compressive strength than 1.5% MSTF, implying that mixed-size fibers can provide more effective suppression of microcrack coalescence under compression through hierarchical bridging and improved stress redistribution, provided that dispersion remains stable. Overall, these results confirm that compressive strength in fiber-reinforced RPC is governed not by fiber volume alone, but by the coupled compatibility between matrix rheology, dispersion quality, and the multi-scale bridging architecture [32].

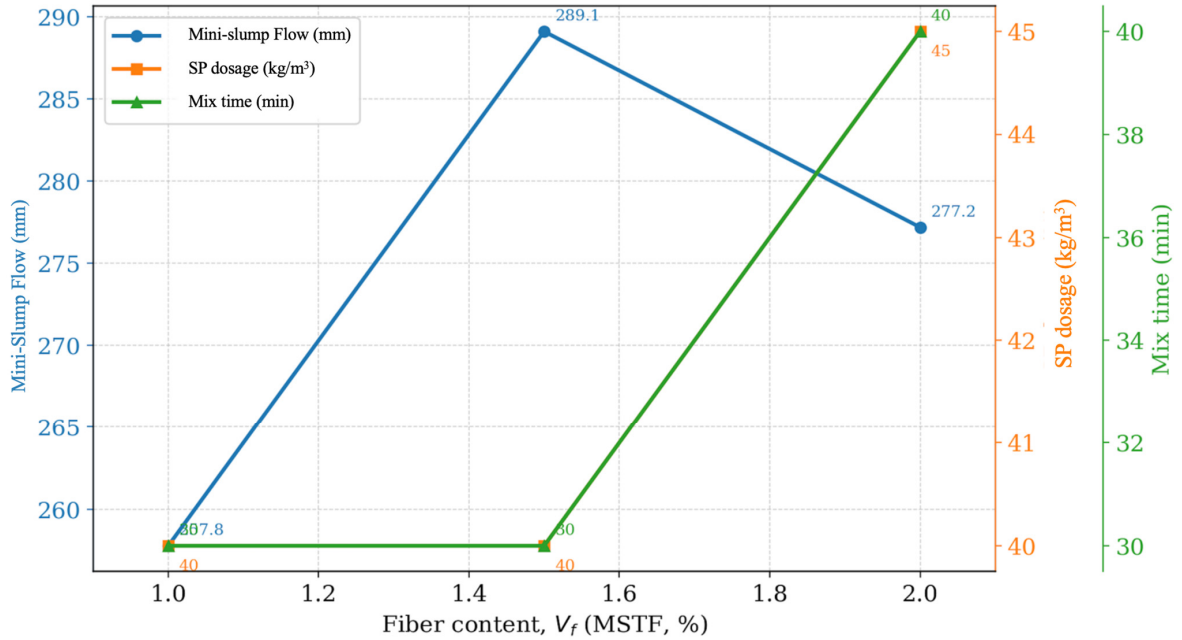


Figure 6. Mini-slump flow, SP dosage, and mix time vs. fiber content of RPC (C66F32S2).

On the contrary, the tensile-related responses (see Figure 8) provide a more direct insight into fiber-bridging mechanisms and reveal why "optimized distribution" can be more important than "more fibers" [33]. For MSTF mixtures, increasing the fiber volume fraction from 1.0% to 2.0% increases flexural strength from 13.14 MPa to 16.53 MPa, consistent with enhanced crack-bridging density under bending. However, the incremental gain from 1.5% to 2.0% is comparatively modest (15.06 → 16.53 MPa), while it requires a substantial increase in fiber consumption and fresh-state demand. In parallel, the 1.5% MSTF mixture exhibits a strong balance between splitting tensile strength (14.94 MPa) and flexural strength (15.06 MPa), with relatively low variability, indicating a more uniform fiber dispersion and more predictable crack evolution.

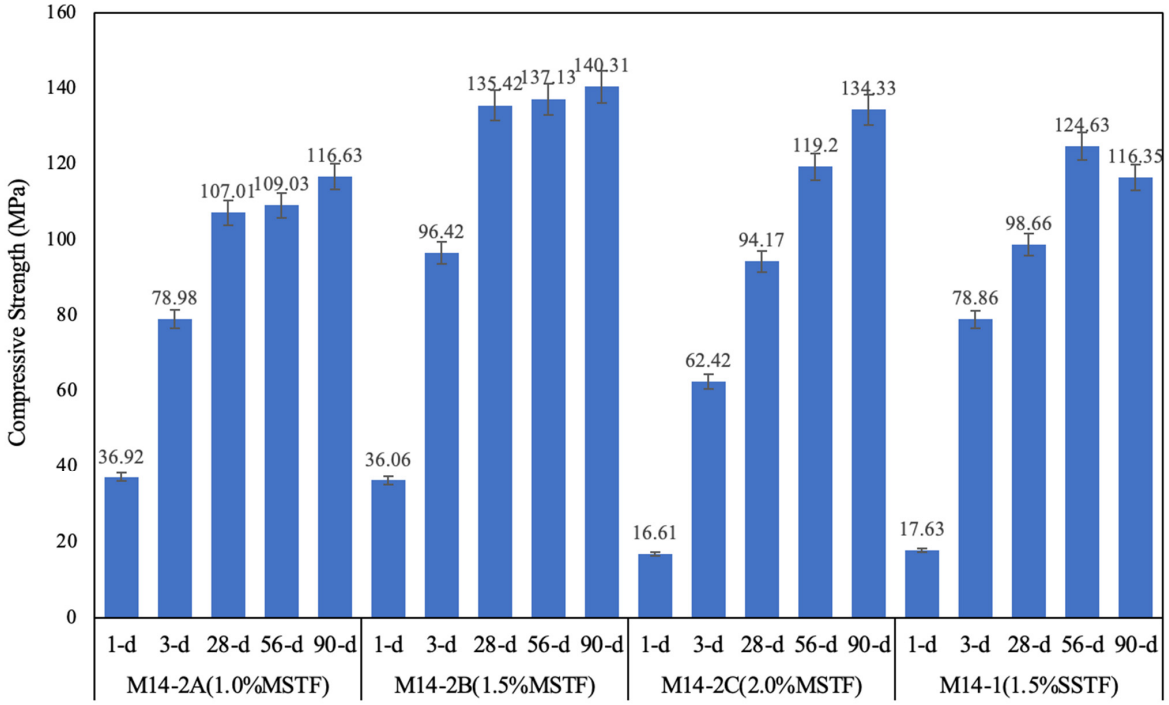


Figure 7. Compressive strength of STF-RPC with various curing times.

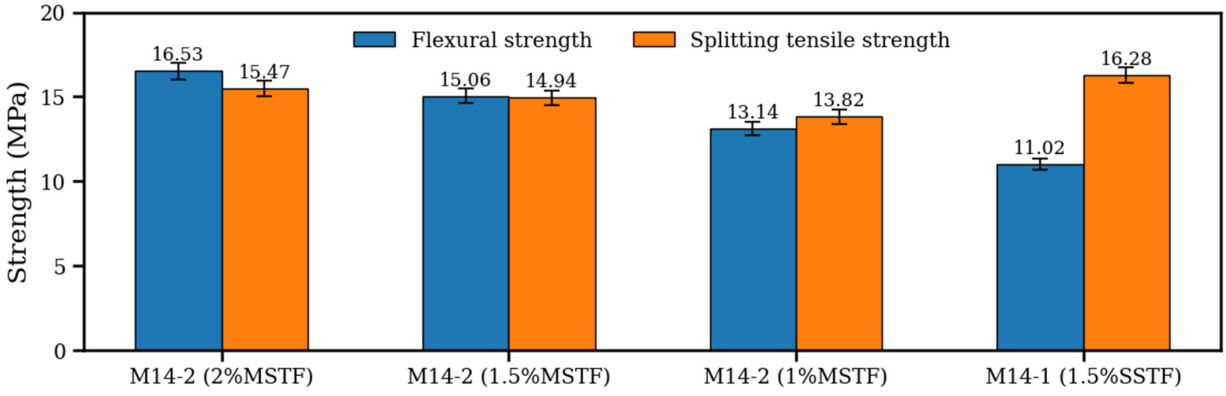


Figure 8. Flexural and splitting tensile strength (28 days).

Notably, the SSTF mixture shows a different signature: it achieves a relatively high splitting tensile strength (16.28 MPa) but a much lower flexural strength (11.02 MPa). This divergence suggests that the single-size fiber system may provide effective resistance under a more uniform tensile stress state (splitting), yet it is less capable of delivering stable multi-scale crack control under flexural loading, where crack opening gradients and localized bridging demands are more pronounced [34]. Mixed-size fibers, by spanning different crack widths and engaging multiple bridging scales, are better suited to sustain load transfer and delay localization under bending. Therefore, the MSTF system offers a more "structurally useful" reinforcement mode for RPC applications where flexural and post-cracking performance govern serviceability and safety.

A consistent mechanistic pattern emerges across binder selection and fiber optimization: the best performance arises from a balance between densification potential and process-induced heterogeneity, rather than from maximizing any single component. At the paste scale, HVFA reduces MWC via micro-filling and improved packing, but the rheological property depends critically on the blended particle size distribution; a small silica fume fraction (around 4% in the ternary systems) can stabilize the flow–water sensitivity and thereby improve the performance under low w/b. At the composite scale, mechanical

performance exhibits a non-monotonic dependence on fiber content: increasing the MSTF content from 1.0% to 1.5% enhances bridging efficiency and improves both compressive development and flexural response, whereas further increasing to 2.0% pushes the system into a dispersion-limited regime, where fiber congestion, higher SP demand, and mixing difficulty promote heterogeneity and undermine strength [35]. This "optimal point" behavior is consistent with mechanistic frameworks emphasizing that ultra-high-performance fiber-reinforced cementitious composites cannot be understood by strength metrics alone; instead, the governing control variable is the coupled stability of crack evolution and fiber bridging under a rheology-constrained situation. In the present study, a 1.5% MSTF content within the HVFA-based low-carbon matrix (Mix No. 14) represents the most efficient balance—maximizing multi-scale bridging effectiveness while maintaining sufficient fresh-state property—thereby enabling 130 MPa class performance without reverting to a high-clinker, high-silica fume, or excessively high-fiber content.

3.3. Durability Assessment

Durability-related transport tests consistently demonstrate that the high-volume fly ash RPC reinforced with 1.5% mixed-size micro steel fibers (Mix No. 14) possesses an exceptionally dense and impermeable microstructure. The RCPT results (see Table 4) obtained in accordance with ASTM C1202 show a charge-passed ranging from 688 to 1066 C at 28 days, with an average of 917.5 C. Based on the ASTM C1202 penetrability classification, these values fall predominantly within the "Very Low" chloride ion penetrability range (100–1000 C), with the maximum value (1066 C) only marginally entering the "Low" category (1000–2000 C) [26]. The overall low electrical response under a constant 60 V potential indicates a highly resistive transport network, which is consistent with the packing-optimized, low-w/b binder matrix and the micro-filling and later-age pozzolanic contributions of class-F fly ash that collectively refine pores and reduce connectivity. Minor specimen-to-specimen variation is expected due to inherent heterogeneity and test-condition sensitivity, while the narrow data band indicates that the mix design provides superior chloride resistance [36]. It is also noted that RCPT is an electrical migration-based index and may be affected by pore solution chemistry in addition to pore structure; nevertheless, the uniformly low charge-passed values suggest that the measured response is governed primarily by microstructural densification rather than by conductive artifacts.

Table 4. RCPT results of M14-2 (1.5%MSTF).

Parameter	Sample 1	Sample 2	Sample 3	Sample 4
Actual Voltage (V)	60	60	60	60
Actual Current (mA)	34.5	47.8	43.3	50.8
Temperature (°C)	27.5	27.9	29.7	29
Time (h)	6	6	6	6
Pred. Coulombs (adjusted)	688	1022	894	1066
Avg. Coulombs	917.5			
Permeability Class	Very Low			

The excellent chloride resistance is consistent with the proposed mix design strategy that couples particle packing optimization with low-w/b rheology control. A densely packed granular skeleton reduces initial interparticle voids and disrupts the continuity of capillary pathways, while the micro-filler effect of ultra-fine constituents and the later-age pozzolanic reaction of class-F fly ash further refine the pore structure and increase tortuosity, thereby suppressing ionic transport. The relatively narrow scatter among replicate specimens suggests that the optimized formulation provides robust resistance to chloride

ingress despite the inherent heterogeneity of fiber-reinforced cementitious composites and the sensitivity of migration-based tests to specimen conditioning.

It should be noted that RCPT is an electrical migration index and may be influenced not only by pore geometry but also by pore solution chemistry (e.g., ionic concentration and conductivity) [26]. Nonetheless, the consistently low charge-passed values observed in this study strongly suggest that the measured response is governed primarily by microstructural densification and reduced pore connectivity, rather than by conductive artifacts.

To further substantiate the "binder packing optimization" discussed, the particle packing state of the optimized low-carbon FR-RPC was evaluated using the Modified Andreasen and Andersen (MMA) model (see Figure 9), following the validation logic commonly adopted in MMA-based mixture design studies (i.e., fitting the mixture grading to an MMA target curve and reporting goodness-of-fit indices) [37,38]. The MMA target cumulative grading is expressed as shown in Equation (1):

$$P(D) = \frac{D^q - D_{\min}^q}{D_{\max}^q - D_{\min}^q} \quad (1)$$

where D_{min} and D_{max} denote the minimum and maximum particle sizes considered, and q is the distribution modulus controlling the slope of the target curve [37,38]. In this study, D_{min} and D_{max} were defined as the smallest particle size of the finest binder constituent and the largest particle size of the fine aggregate fraction used in the RPC matrix, respectively. The distribution modulus was set to q = 0.28 to target a dense RPC-type skeleton while maintaining adequate rheological tolerance for uniform fiber dispersion [37].

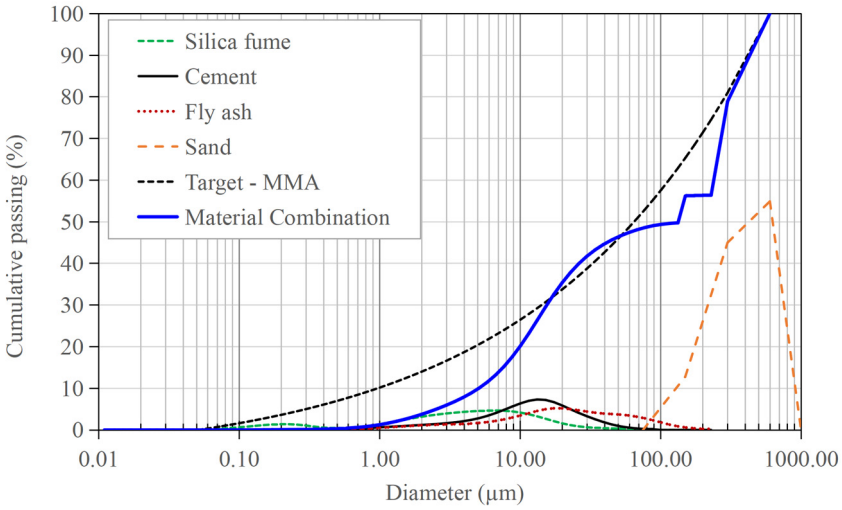


Figure 9. Particle size distribution of the material blend compared with the target curve, as predicted by MMA theory.

The agreement between the measured mixture grading and the MMA target curve was quantified using the root sum of squares (RSS) and the coefficient of determination (R^2) as shown in Equations (2) and (3) [38]:

$$RSS = \sum_{i=1}^{n} [P_{mix}(D_i) - P_{tar}(D_i)]^2 \quad (2)$$

$$R^2 = 1 - \frac{\sum_{i=1}^{n} [P_{mix}(D_i) - P_{tar}(D_i)]^2}{\sum_{i=1}^{n} [P_{mix}(D_i) - \overline{P}_{mix}]^2} \quad (3)$$

where P_{mix} and P_{tar} represent the cumulative passing fractions of the actual mixture and the MMA target curve, respectively [38]. Based on the measured PSDs of cement, class-F fly ash, silica fume, and the selected river sand gradation, together with the optimized volumetric proportions, the assembled mixture grading yields RSS = 0.359 (cumulative fractions normalized to 0–1) and R^2 = 0.906. These indices indicate a close match between the designed grading and the MMA target distribution, confirming that the adopted binder–sand system approaches an MMA-optimized packing state [37,38]. From a transport standpoint, an MMA-consistent grading reduces interparticle voids and promotes a more continuous and compact granular skeleton, thereby lowering the connectivity of permeable pores after hydration—consistent with the observed low RCPT charge passed and the accompanying water absorption performance.

Finally, it should be emphasized that MMA-based packing optimization is necessary but not sufficient to maximize performance in cementitious materials. While MMA indices quantify geometric compactness, the ultimate durability response also depends on dispersion quality (particularly for silica fume), water demand, rheology-controlled entrapped air/voids, and the extent of later-age pozzolanic reactions in high-volume fly ash systems [37]. Accordingly, MMA fitting (high R^2 and low RSS) is employed here as a quantitative validation of "binder packing optimization," whereas the consistently low chloride penetrability and low water absorption are achieved through the combined framework of packing density optimization and paste rheology optimization, which ensures both microstructural densification and practical workability for stable fiber dispersion.

Complementary permeability assessment via water absorption further confirms the same transport-resistant signature. Mix No. 14 exhibits extremely low capillary uptake, with initial sorptivity in the order of 10^{-3} mm·s$^{-1/2}$, i.e., substantially lower than typical values reported for conventional and many high-performance concretes [39]. The uptake curves show strong linearity ($R^2 > 0.98$) and limited scatter among replicates, reflecting both a stable testing response and a highly homogeneous material system (see Table 5 and Figure 10). This superior resistance to capillary ingress is attributed to the ultra-low w/b ratio and the highly compact, discontinuous pore network achieved through binder packing optimization, while micro steel fibers help preserve this impermeability by limiting microcrack initiation and restraining crack opening, thereby preventing the formation of connected transport pathways (see Figure 11).

Table 5. Water absorption rate results of M14-2 (1.5%MSTF).

Parameters		Sample 1	Sample 2	Sample 3	Sample 4
Initial Sorptivity ($mm/\sqrt{s}$)	Standard Requirement		<0.01		
	Test Result	0.0019	0.0018	0.0014	0.0019
Secondary Sorptivity ($mm/\sqrt{s}$)	Standard Requirement		<0.01		
	Test Result	0.0007	0.0007	0.0007	0.0007
R^2 correlation Coefficient	Standard Requirement		>0.98		
	Initial Sorptivity	0.9873	0.9858	0.985	0.9842
	Secondary Sorptivity	0.9841	0.9841	0.9819	0.9902
Status		PASS	PASS	PASS	PASS

Specifically, it shows that specimens with a 1.5% MSTF content exhibit a relatively intact matrix–fiber interface with fewer visible microcracks and a relatively dense matrix surrounding the fibers, indicating effective crack bridging and good fiber–matrix bonding. In contrast, increasing the fiber dosage to 2.0% results in more pronounced local defects around fibers, including interfacial microcracking and debonding features, which can be largely attributed to reduced workability and greater difficulty in fiber dispersion. Such

superior resistance to capillary ingress is mainly ascribed to the ultra-low w/b ratio and the highly compact, discontinuous pore network formed via binder packing optimization. Moreover, micro steel fibers at an appropriate dosage help maintain impermeability by restricting microcrack initiation and restraining crack opening, thus avoiding the formation of connected transport pathways. These microstructural observations confirm that steel fibers can effectively suppress crack propagation and preserve impermeability when used at an optimal content, whereas excessive fiber dosage may introduce local discontinuities caused by insufficient dispersion and stress concentration. Therefore, an optimized fiber content is critical to achieving a favorable balance between mechanical performance improvement and transport resistance enhancement.

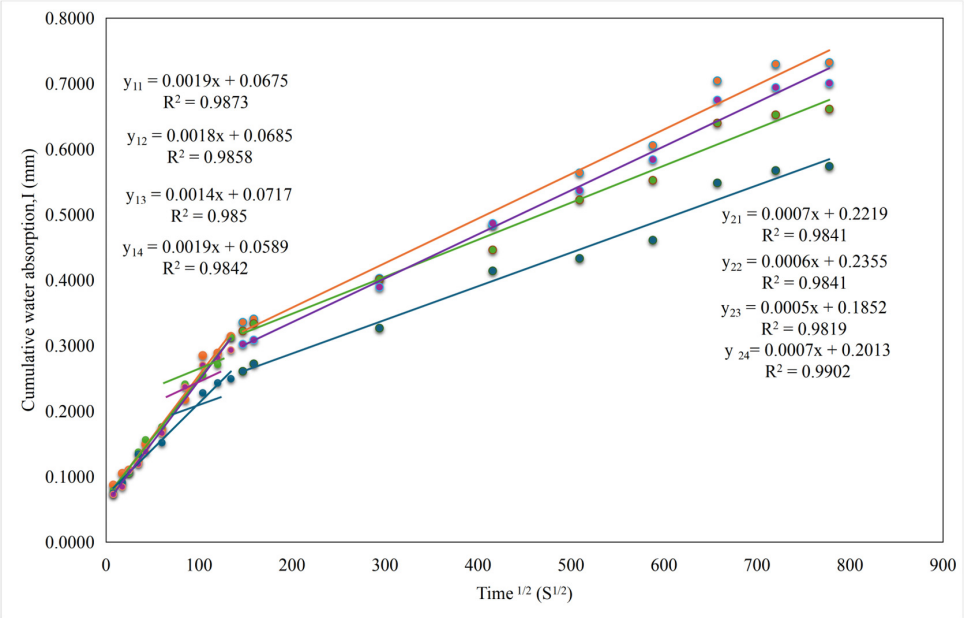


Figure 10. Fitting curves of the sorptivity of the samples of M14-2 (1.5%MSTF).

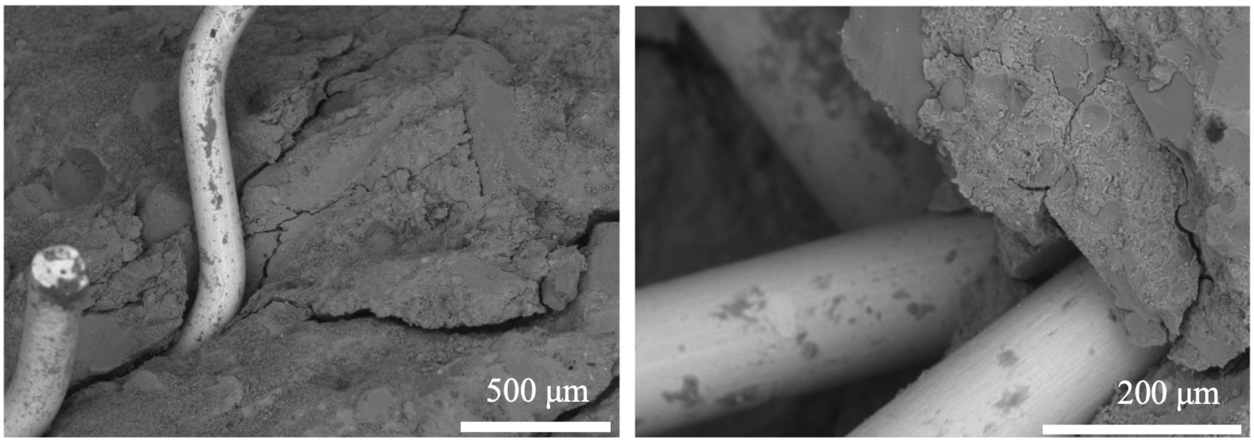


Figure 11. Micrograph of samples with 1.5% MSTF (**left**); and 2% MSTF (**right**).

3.4. Environmental Assessment

The environmental assessment of the developed RPC mixtures was quantified using total embodied CO_2, together with a strength-normalized carbon index (CI), defined as the embodied CO_2 per unit volume divided by the 28-day compressive strength (kg $CO_2 \cdot kg^{-1} \cdot MPa^{-1}$). As shown in Figure 12, all redesigned mixtures exhibit a clear reduction in embodied CO_2 relative to the reference RPC. Specifically, the reference mixture

shows the highest total CO_2 of 1014 kg CO_2/kg, whereas the Mix No. 14 series reduces total CO_2 to 693–814 kg CO_2/kg, with the minimum recorded for M14-2A (1.0% MSTF) at 693 kg CO_2/kg (≈31.7% lower than the reference). This improvement is primarily driven by the binder redesign that substantially reduces clinker-based constituents and silica fume demand, thereby lowering the dominant emission contributions typically associated with conventional RPC. While steel fibers remain an important contributor whose impact scales directly with dosage, and the higher superplasticizer requirement at low w/b inevitably increases admixture-related emissions (see Table 6), these increases are outweighed by the reductions achieved through clinker and silica fume replacement.

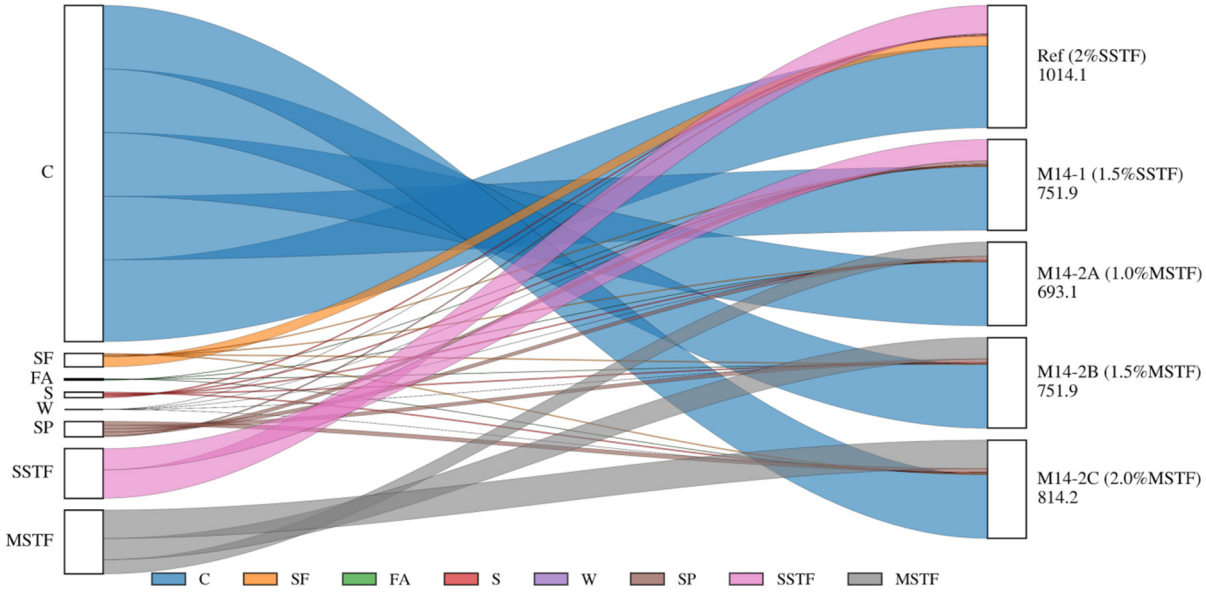


Figure 12. RPC mixtures: Material-wise embodied CO_2 contribution (kg CO_2 per kg).

Table 6. Carbon emission factor of all components.

Material	Emission Factor (kg CO_2/kg)	Ref.
C	0.724	[18]
S	0.01	[40]
SF	0.354	[41]
W	0.0003	[40]
SP	0.72	[40]
SSTF	1.4965	[40]
MSTF	1.4965	-
FFA	0.009	[42]

Importantly, Figure 13 demonstrates why strength-normalized assessment is essential for identifying the truly sustainable formulation. Although M14-2A exhibits the lowest total CO_2, its overall carbon efficiency is not optimal once mechanical performance is accounted for, yielding a CI of 6.48. In contrast, M14-2B (1.5% MSTF) achieves the lowest CI (5.55)—a 31.7% reduction relative to the reference (8.13)—because its superior 28-day compressive strength offsets its higher total CO_2 (752 kg CO_2/kg) compared with M14-2A. This indicates that the most sustainable RPC is not necessarily the mixture with the minimum embodied CO_2, but the one that delivers the best performance per unit carbon. Conversely, increasing the fiber dosage to 2.0% MSTF (M14-2C) results in a CI of 8.65, which exceeds the reference despite a reduced total CO_2 (814 kg CO_2/kg). This outcome is consistent with the previously observed non-monotonic fiber effect: excessive fiber content

increases material-related emissions and can degrade workability and dispersion quality, which penalizes compressive strength and therefore worsens strength-normalized carbon efficiency [43]. Overall, the environmental assessment results confirm that the proposed low-carbon design strategy can meaningfully reduce environmental burden and that the 1.5% MSTF configuration provides the most favorable carbon–strength synergy, effectively decoupling 130 MPa class performance from high embodied emissions.

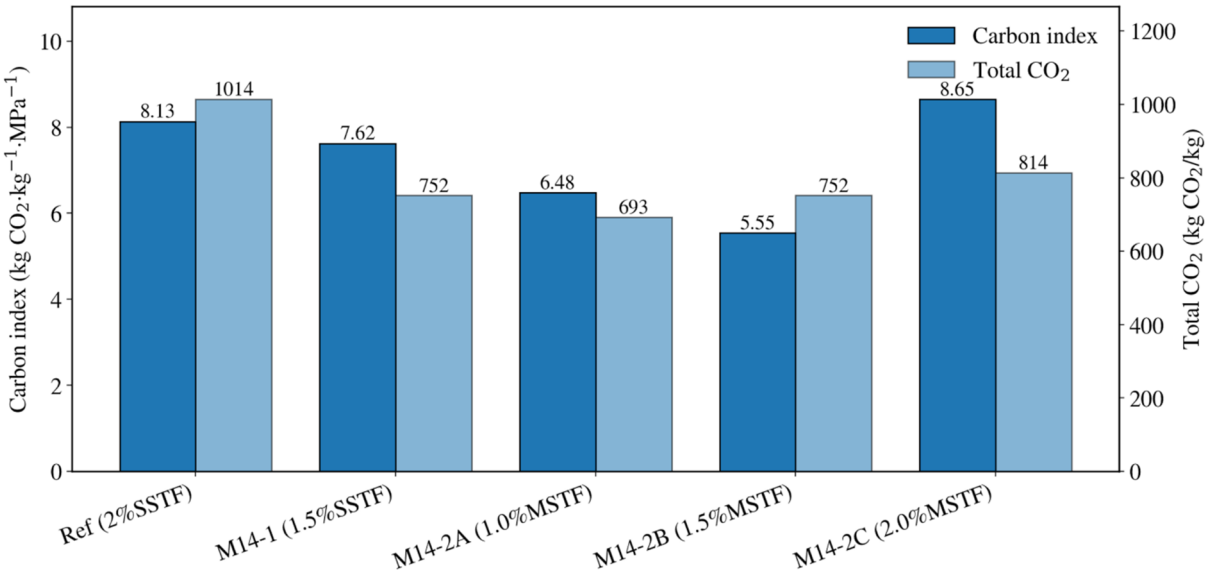


Figure 13. Carbon index and carbon intensity.

4. Conclusions

This study systematically optimized a low-carbon RPC incorporating high-volume class-F fly ash and mixed-size steel fibers, and comprehensively assessed its mechanical performance, durability, and environmental impact. The following conclusions can be drawn:

1. A cost-effective and low-carbon RPC matrix was successfully developed by substantially reducing cement and silica fume contents and incorporating high-volume class-F fly ash while maintaining dense particle packing and adequate rheological performance. Among the binder systems investigated, Mix No. 14 exhibited the most balanced overall performance and was therefore selected as the optimal reference matrix for subsequent fiber optimization.
2. MSTF significantly improved the tensile-related performance and overall mechanical synergy of RPC. An optimal fiber volume fraction of 1.5% was identified, delivering the best balance among compressive, splitting tensile, and flexural strengths, together with a good workability and low result scatter. Increasing the fiber content to 2.0% provided diminishing or even adverse returns, which is attributed to fiber crowding, impaired dispersion, and the associated degradation of mixture stability and load-transfer efficiency.
3. Durability-related transport tests confirmed the exceptional impermeability of the optimized low-carbon RPC. The 1.5% MSTF mixture showed a very low chloride ion penetrability (RCPT charge passed predominantly within the “Very Low” range) and an extremely low sorptivity, indicating a highly compact, weakly connected pore network and a strong resistance to water and ion ingress. These results support its suitability for long-term service in aggressive environments where chloride attack and moisture transport govern durability.

4. The superior macroscopic performance of the optimized mixtures is mechanistically consistent with a densified matrix and effective fiber–matrix interaction. The mixed-size fiber system promotes multi-scale crack bridging, improving stress redistribution and restraining crack opening while maintaining a relatively uniform dispersion, thereby enhancing both strength and performance stability.
5. The environmental assessment results demonstrate that all of the optimized mixtures achieve a substantial reduction in embodied carbon relative to the reference RPC, with CO_2 intensity decreasing markedly and overall emissions reduced by approximately 20.4–31.6%. This improvement is primarily driven by the drastic reduction of clinker-based constituents and silica fume, confirming that ultra-high performance can be achieved alongside meaningful decarbonization when the binder system is packing- and rheology-optimized.

Author Contributions: Y.P.: Methodology, Investigation, Writing—original draft, Formal analysis; N.C.: Methodology, Writing—review and editing, Supervision, Funding acquisition; Y.W., and Y.C.: Writing—review and editing; K.C.: Conceptualization, Methodology, Validation, Writing—review and editing, Supervision, Funding acquisition. All authors have read and agreed to the published version of the manuscript.

Funding: This research and the APC were funded by Mahasarakham Universiy, Thailand.

Data Availability Statement: The data presented in this study are available on request.

Acknowledgments: This research project was financially supported by Mahasarakham University, Thailand.

Conflicts of Interest: The authors declare that they have no known competing financial interests or personal relationships that could have appeared to influence the work reported in this paper.

References

1. Ullah, R.; Qiang, Y.; Ahmad, J.; Vatin, N.I.; El-Shorbagy, M.A. Ultra-High-Performance Concrete (UHPC): A State-of-the-Art Review. *Materials* **2022**, *15*, 4131. [CrossRef] [PubMed]
2. Nasr, M.S.; Hasan, Z.A.; Jaaz, H.A.G.; Abed, M.K.; Falah, M.W.; Hashim, T.M. Mechanical properties of sustainable reactive powder concrete made with low cement content and high amount of fly ash and silica fume. *J. Mech. Behav. Mater.* **2022**, *31*, 617–622. [CrossRef]
3. Ge, W.; Wang, A.; Zhang, Z.; Ge, Y.; Chen, Y.; Li, W.; Jiang, H.; Shuai, H.; Sun, C.; Yao, S.; et al. Study on the workability, mechanical property and water absorption of reactive powder concrete. *Case Stud. Constr. Mater.* **2023**, *18*, e01777. [CrossRef]
4. da Silva, M.L.; Prado, L.P.; Félix, E.F.; de Sousa, A.M.D.; Aquino, D.P. The Influence of Materials on the Mechanical Properties of Ultra-High-Performance Concrete (UHPC): A Literature Review. *Materials* **2024**, *17*, 1801. [CrossRef] [PubMed]
5. Odorčić, N.B.; Kravanja, G. Combined Effects of Metakaolin and Hybrid Fibers on Self-Compacting Concrete. *Materials* **2022**, *15*, 5588. [CrossRef]
6. Tang, J.; Gao, C.; Li, Y.; Xu, J.; Huang, J.; Xu, D.; Hu, Z.; Han, F.; Liu, J. A Review on Multi-Scale Toughening and Regulating Methods for Modern Concrete: From Toughening Theory to Practical Engineering Application. *Research* **2024**, *7*, 0518. [CrossRef]
7. Huts, A.; Konkol, J.; Marchuk, V. Granite Dust and Silica Fume as a Combined Filler of Reactive Powder Concrete. *Materials* **2024**, *17*, 6025. [CrossRef]
8. Rong, H.; Sun, W.; Ma, H.; Luo, M.; You, Z.; Zhang, G.; Zhu, P.; Liu, Z.; Gómez-Zamorano, L.Y. Machine Learning-Driven Strength Prediction and Sustainability Analysis of Ultra-High-Performance Concrete. *Materials* **2025**, *18*, 5116. [CrossRef]
9. Liu, W.; Han, J. Fiber Synergy of Polyvinyl Alcohol and Steel Fibers on the Bond Behavior of a Hybrid Fiber-Reinforced Cementitious Composite. *Materials* **2024**, *17*, 629. [CrossRef] [PubMed]
10. Vairagade, V.S. Multi-scale theoretical modeling with molecular simulation framework for fly ash-based high-performance concrete. *Sci. Rep.* **2025**, *15*, 44895. [CrossRef] [PubMed]
11. Zhou, Y.; Elchalakani, M.; Sadakkathulla, M.A.; Hassanli, R.; Guo, X.; Tawfik, E.; Youssf, O. Impact of fly ash on slag-based engineered geopolymer composites: Multiple-scale investigations. *Structures* **2025**, *80*, 109751. [CrossRef]
12. Kumar, B.; Sharma, A.; Ray, S. An analytical approach for characterizing the fracture behaviour of ultra-high-performance fibre reinforced concrete. *Compos. Struct.* **2024**, *324*, 117922. [CrossRef]

13. Hawileh, R.A.; Shaw, S.K.; Assad, M.; Khan, A.A.; Abdalla, J.A. Influence of fly ash on the compressive strength of ultrahigh-performance concrete: A state-of-the-art review towards sustainability. *Int. J. Concr. Struct. Mater.* **2025**, *19*, 25. [CrossRef]
14. Sarmiento-Pupo, K.D.; Escalante-Tovar, J.D.; Altamiranda, J.E.; Abellan-Garcia, J.; Vélez, J.I. Predicting flexural strength in fiber-reinforced UHPC via random forest. *Sci. Rep.* **2025**, *15*, 42045. [CrossRef]
15. *TIS 2594-2556*; Hydraulic Cement. Thai Industrial Standards Institute: Bangkok, Thailand, 2013.
16. Wu, Q.; An, X.H. Development of a mix design method for SCC based on the rheological characteristics of paste. *Constr. Build. Mater.* **2014**, *53*, 642–651. [CrossRef]
17. Solouki, A.; Visintin, P.; Sheikh, A.H. Multi-objective optimization of ultra-high performance concrete using an integrated ANN-based approach. *Constr. Build. Mater.* **2022**, *340*, 127718. [CrossRef]
18. Thai Cement Manufacturers Association. Cement Products Care for the Environment: Hydraulic Cement. Available online: https://www.thaicma.or.th/en/environmentally/environment/environmentally_friendly_cement_products (accessed on 9 June 2024).
19. *ASTM C618*; Standard Specification for Coal Fly Ash and Raw or Calcined Natural Pozzolan for Use in Concrete. ASTM International: West Conshohocken, PA, USA, 2003.
20. *JT/T 524*; Fiber for Cement Concrete in Highway. Ministry of Transport: Beijing, China, 2019.
21. Meng, W.; Valipour, M.; Khayat, K.H. Optimization and performance of cost-effective ultra-high performance concrete. *Mater. Struct.* **2017**, *50*, 29. [CrossRef]
22. *ASTM C1437*; Standard Test Method for Flow of Hydraulic Cement Mortar. ASTM International: West Conshohocken, PA, USA, 2001.
23. *ASTM C109*; Standard Test Method for Compressive Strength of Hydraulic Cement Mortars. ASTM International: West Conshohocken, PA, USA, 2002.
24. *ASTM C496*; Standard Test Method for Splitting Tensile Strength of Cylindrical Concrete Specimens. ASTM International: West Conshohocken, PA, USA, 2004.
25. *ASTM C78*; Standard Test Method for Flexural Strength of Concrete (Using Simple Beam with Third-Point Loading). ASTM International: West Conshohocken, PA, USA, 2002.
26. *ASTM C1202*; Standard Test Method for Electrical Indication of Concrete's Ability to Resist ChlorideIon Penetration. ASTM International: West Conshohocken, PA, USA, 1997.
27. *ASTM C1585*; Standard Test Method for Measurement of Rate of Absorption of Water by Hydraulic Cement Concretes. ASTM International: West Conshohocken, PA, USA, 2013.
28. Ojala, T.; Chen, Y.; Punkki, J.; Al-Neshawy, F. Characteristics of Entrained Air Voids in Hardened Concrete with the Method of Digital Image Analysis Coupled with Schwartz-Saltykov Conversion. *Materials* **2021**, *14*, 2439. [CrossRef] [PubMed]
29. Khayat, H.K.; Kassimi, F.; Ghoddousi, P. Mixture design and testing of fiber-reinforced self-consolidating concrete. *ACI Mater. J.* **2014**, *111*, 143–152.
30. Farrant, W.E.; Babafemi, A.J.; Kolawole, J.T.; Panda, B. Influence of Sugarcane Bagasse Ash and Silica Fume on the Mechanical and Durability Properties of Concrete. *Materials* **2022**, *15*, 3018. [CrossRef]
31. Zhao, S.; Bo, Y. Effect of Casting Position on Mechanical Performance of Ultra-High Performance Concrete. *Materials* **2022**, *15*, 404. [CrossRef] [PubMed]
32. Chen, Y.; Waheed, M.S.; Iqbal, S.; Rizwan, M.; Room, S. Durability Properties of Macro-Polypropylene Fiber Reinforced Self-Compacting Concrete. *Materials* **2024**, *17*, 284. [CrossRef]
33. Choi, M.S.; Kang, S.-T.; Lee, B.Y.; Koh, K.-T.; Ryu, G.-S. Improvement in Predicting the Post-Cracking Tensile Behavior of Ultra-High Performance Cementitious Composites Based on Fiber Orientation Distribution. *Materials* **2016**, *9*, 829. [CrossRef]
34. Yang, K.; Huang, W.; Sun, M.; Zheng, Z.; Lin, H. Effect of Fiber Characteristics on Cracking Resistance Properties of Stone Mastic Asphalt (SMA) Mixture. *Polymers* **2025**, *17*, 2623. [CrossRef]
35. Ashokan, A.; Rajendran, S.; Dhairiyasamy, R. A comprehensive study on enhancing of the mechanical properties of steel fiber-reinforced concrete through nano-silica integration. *Sci. Rep.* **2023**, *13*, 20092. [CrossRef]
36. Yang, Y.; Takasu, K.; Suyama, H.; Ji, X.; Xu, M.; Liu, Z. Comparative Analysis of Woody Biomass Fly Ash and Class F Fly Ash as Supplementary Cementitious Materials in Mortar. *Materials* **2024**, *17*, 3723. [CrossRef]
37. Niewiadomski, P.; Szymanowski, J.; Karolak, A.; Sadowski, Ł.; Stefaniuk, D.; Królicka, A. Cement Paste Mixture Proportioning with Particle Packing Theory: An Ambiguous Effect of Microsilica. *Materials* **2021**, *14*, 6970. [CrossRef]
38. Xie, B.-X.; Wang, S.; Zhang, X.-E.; Luo, R.-H.; Chen, G.; Xie, Z.-H.; Lin, J.-X. Dynamic Mechanical Properties and a Predictive DIF Model of Seawater-Coral Sand ECC: Effects of Water-to-Binder and Sand-to-Binder Ratios. *Constr. Build. Mater.* **2026**, *507*, 145059. [CrossRef]
39. Malaiškienė, J.; Jakubovskis, R. Influence of Pozzolanic Additives on the Structure and Properties of Ultra-High-Performance Concrete. *Materials* **2025**, *18*, 1304. [CrossRef]

40. Tran, T.M.; Trinh, H.T.; Nguyen, D.; Tao, Q.; Mali, S.; Pham, T.M. Development of sustainable ultra-high-performance concrete containing ground granulated blast furnace slag and glass powder: Mix design investigation. *Constr. Build. Mater.* **2023**, *397*, 132358. [CrossRef]
41. Moula, S.; Fraj, A.B.; Wattez, T.; Bouasker, M.; Ali, N.B.H. Mechanical properties, carbon footprint and cost of ultra-high performance concrete containing ground granulated blast furnace slag. *J. Build. Eng.* **2023**, *79*, 107796. [CrossRef]
42. Liu, Z.; Fang, M.; Jiao, Y.; Chen, Y.; Yang, H.; Wu, Q. Acoustic Emission–Based Shear Fracture Characterization of Ultra-High-Performance Concrete with Varying Steel Fiber Contents. *Fatigue Fract. Eng. Mater. Struct.* **2025**, *48*, 580–598. [CrossRef]
43. Khan, M.I.; Abbass, W.; Alrubaidi, M.; Alqahtani, F.K. Optimization of the Fine to Coarse Aggregate Ratio for the Workability and Mechanical Properties of High Strength Steel Fiber Reinforced Concretes. *Materials* **2020**, *13*, 5202. [CrossRef] [PubMed]

Disclaimer/Publisher's Note: The statements, opinions and data contained in all publications are solely those of the individual author(s) and contributor(s) and not of MDPI and/or the editor(s). MDPI and/or the editor(s) disclaim responsibility for any injury to people or property resulting from any ideas, methods, instructions or products referred to in the content.